Asymmetric cation nonstoichiometry in spinels: Site occupancy in Co_2ZnO_4 and Rh_2ZnO_4

Tula R. Paudel,[1] Stephan Lany,[1] Mayeul d'Avezac,[1] Alex Zunger,[1] Nicola H. Perry,[2] Arpun R. Nagaraja,[2] Thomas O. Mason,[2] Joanna S. Bettinger,[3] Yezhou Shi,[3,4] and Michael F. Toney[3]

[1]*National Renewable Energy Laboratory, Golden, Colorado 80401, USA*

[2]*Northwestern University, Evanston, Illinois 60208, USA*

[3]*SLAC National Accelerator Laboratory, Menlo Park, California 94025, USA*

[4]*Stanford University, Stanford, California 94305, USA*

(Received 13 April 2011; published 22 August 2011)

Two cations A and B in A_2BO_4 spinels appear in precise 2:1 Daltonian ratio ("line compounds") only at very low temperature. More typically, at finite temperature, they tend to become either A rich or B rich. Here we survey the experimentally observed stoichiometry asymmetries and describe the first-principles framework for calculating these. Defect calculations based on first principles are used to calculate the enthalpies of substitution of A atom $\Delta H(A_{T_d})$ and B atom $\Delta H(B_{O_h})$ and determine their site occupancies leading to (non)-stoichiometry. In Co_2ZnO_4, the result of the calculation for site occupancy compares well with that measured via anomalous x-ray diffraction. Further, the calculated phase boundary also compares well with that measured via Rietveld refinement of x-ray diffraction data on bulk ceramic sintered samples of Co_2ZnO_4 and Rh_2ZnO_4. These results show that Co_2ZnO_4 is heavily Co nonstoichiometric above 500 °C, whereas Rh_2ZnO_4 is slightly Zn nonstoichiometric. We found that, in general, the calculated $\Delta H(A_{T_d})$ is smaller than $\Delta H(B_{O_h})$, if the A-rich competing phase is isostructural with the A_2BO_4 host, for example, A_2AO_4, whereas B-rich competing phase is not, for example, BO. This observation is used to qualitatively explain nonstoichiometry and solid solutions observed in other spinels.

DOI: 10.1103/PhysRevB.84.064109 PACS number(s): 61.50.Nw, 61.72.J−, 64.75.Nx, 29.20.dk

I. INTRODUCTION

Nonstoichiometry as a theme in inorganic compounds. Binary or ternary inorganic compounds are stoichiometric at low temperature but can become nonstoichiometric upon raising the temperature, thereby changing their electrical, optical, and mechanical properties. Nonstoichiometry often tends to favor a particular atom in a compound. Such preferences are a theme of this paper in the context of spinels. *Binary* compounds such as Cu_2O (Ref. 1) and NiO (Ref. 2), tend to become cation-deficient and p-type, whereas ZnO is anion deficient,[2,3] as are the transition-metal carbides [TiC, ZrC, NbC, WC (Ref. 4)] and nitrides [TiN (Ref. 5)]. Vacancies in such carbides often cause lattice distortion, thereby changing their mechanical, magnetic, superconducting, and catalytic properties.[6]

Ternary two-cation compounds such as spinels [A_2BO_4 (Ref. 7)] offer the possibility of cation-A vs cation-B nonstoichiometry as opposed to only cation vs anion nonstoichiometry in binary compounds. As seen schematically in Fig. 1 cation A vs B nonstoichiometry in a spinel x-T phase diagram appears as the phase boundary (a) leaning toward A, leaning toward B, leaning toward both A and B often at different temperatures and pressures, and remaining completely stoichiometric. Examination of the measured phase-diagrams of such spinels[10] demonstrates specific asymmetry in cation nonstoichiometry as shown in Fig. 2. For example, some spinels such as Cr_2MgO_4, Cr_2FeO_4, Cr_2MnO_4, and Al_2FeO_4 permit an *excess* of low-valent cation B, while other spinels such as Co_2ZnO_4, Ga_2CdO_4, Fe_2CuO_4, and Co_2NiO_4, become *deficient* in low-valent cation B; still other spinels such as Al_2MgO_4 and Mn_2CuO_4 allow an excess in both cations A and B at different temperatures and pressures.

Nonstoichiometry reflecting preference for the site occupancies. Microscopically, (non)-stoichiometry, in general, reflects preference of site occupancy, which is controlled by the enthalpy of formation of A and B cations on available lattice sites. Spinel is a cubic crystal, in which Wyckoff positions 8a [tetrahedral (T_d) site] and 16d [octahedral (O_h) site] are occupied by cations A or B and 32e is occupied by oxygen. Depending upon the site occupancies of the A and B atoms at low temperatures, spinel is called either (ordered)-normal ($Fd3m$) or (ordered)-inverse ($P4_122$).[11] In (ordered)-normal spinel, at low temperatures, A atoms occupy O_h sites and B atoms occupy T_d sites, while in (ordered)-inverse spinels A atoms occupy all T_d sites and 50% of O_h sites, whereas B atoms occupies the rest of the O_h sites. Both of these cases represent a single configuration: "Each atom occupies only one possible site (hence no configurational entropy)." As the temperature rises, there are two different channels of disorder. *First* is the configurational disorder with perfect stoichiometry. In this case, the A:B:O ratio is still 2:1:4 but cation site occupancies are swapped between O_h and T_d as described by the general formula $[A_{(2-\lambda)}\mathbf{B}_\lambda](\mathbf{A}_\lambda B_{(1-\lambda)})O_4$ with an inversion parameter ($0 \leqslant \lambda \leqslant 1$). The value of λ defines the degree of inversion and [square] (round) brackets denote [octahedral] (tetrahedral) sites. This configurational entropy effect causes one of following two order-disorder phase transitions depending on the starting configuration[12]: (a) continuous transition between ordered-normal to disordered-dual [both $Fd3m$ but λ increases from zero toward 2/3 creating B_{O_h} and A_{T_d})], or first order transition from ordered-inverse ($P4_122$) to disordered-inverse [$Fd3m$ (λ stays 1 but occupancy of O_h sites get randomized)], followed by continuous phase transition form the disordered-inverse to disordered-dual (both $Fd3m$ but λ decreases from 1 toward 2/3). *Second* is the change of stoichiometry where the A:B:O ratio is altered from 2:1:4. Electrostatically, when the A:O charge balance in binary oxides such as ZrO_2 (Ref. 4) is changed by

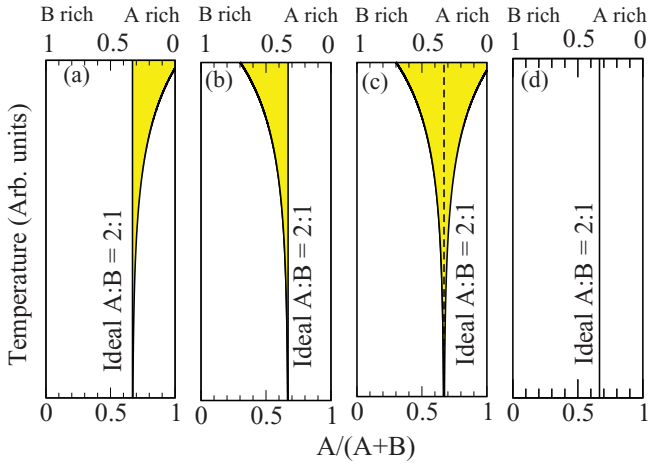

FIG. 1. (Color online) Schematic representation of cation non-stoichiometry in typical phase diagrams of a two-cation (A,B) plus anion compound. The shaded areas represent the stability range of the compound under consideration.

nonstoichiometry, then the system maintains charge neutrality by spontaneously creating oxygen vacancies. However, in spinels such as Fe_3O_4 (Refs. 13 and 14) and others[15–18] both cation and anion vacancies and cation interstitials formation energies are much larger than for antisites defects formation; that is, these are minority defects vis-à-vis antisite defects insofar as cation nonstoichiometry and charge balance is concerned (although they remain important for cation diffusion). This paper focuses on the difference in antisite occupancies being the primary cause of nonstoichiometry in spinels.

Antisites occupancies depend on the antisites heats of formation (see Fig. 3). Large heat of formation means a small number of defects and vice versa. Thus, for the pronounced nonstoichiometry toward A, for example for a normal spinel, one requires a small $H(A_{T_d})$ and relatively larger B_{O_h}, and for pronounced nonstoichiometry toward B, one requires a small B_{O_h} and relatively larger A_{T_d}. On the other hand, if A_{T_d} and B_{O_h} are similar and small one expects negligible nonstoichiometry, and most of the disorder will be accommodated by stoichiometric configurational changes (channel *first* above).

The antisites heats of formation in a compound depend on equilibrium phases that are in equilibrium with it (competing phases). In terms of supercell defect-methods terminology, the compound and competing phases form the system and reservoirs, and creation of antisites defects in thermodynamic equilibrium, involve interchanging cations between them. For example, creation of A_{T_d} (A_B) involves taking out original occupants of a T_d site, that is, B atom and putting it to the reservoir and taking A atoms from the reservoir and putting back in T_d sites. Thus, when system and reservoir are similar, then energy required in this process is small; that is, the heat of formation is small. Thus, if the system A_2BO_4 has competing phases such as A_2AO_4 and BO, $\Delta H(A_{T_d})$ would be smaller than $\Delta H(B_{O_h})$.

Occupancy of antisites, whether the end result is nonstoichiometry or inversion, plays an important role in determining the electrical nature of a compound. For example, in case of a III-II spinel, where the oxidation state of A is 3+ and B is 2+, A_{T_d} (can) lead to an excess of electrons where as a low valent cation B_{O_h} (can) lead to an excess of holes, a process

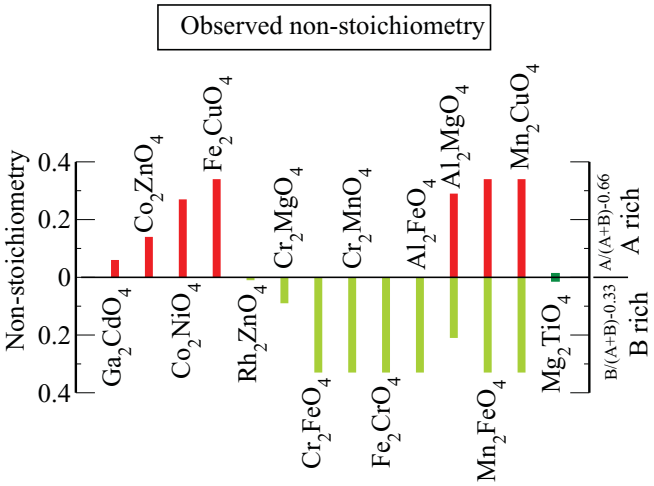

FIG. 2. (Color online) Maximum A vs B cation non-stoichiometry observed in various compounds found in the NIST phase diagram collection (Ref. 10). The compounds with only a red bar are non-stoichiometric toward A, whereas those with only yellowish green bars are non-stoichiometric toward B, and those with both red and yellowish green bars are non-stoichiometric toward both A and B, often under different conditions, and the compound with a dark green bar is stoichiometric. Note that A and B non-stoichiometry are defined as $\{[A/(A+B)]-2/3\}$ and $\{[B/(A+B)]-1/3\}$, respectively.

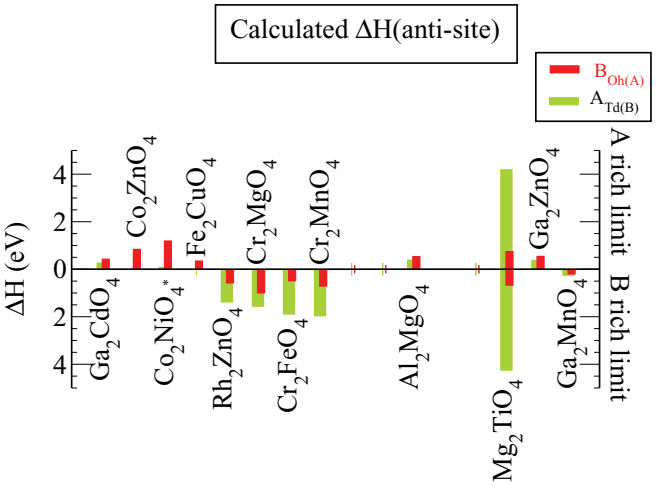

FIG. 3. (Color online) Enthalpy of substitution of energetically dominant charge states of A_{T_d} site and Boh site at the A-rich limit in positive axis and the B-rich limit in negative axis. (Information about dominant charge defects is given in the text.) Compounds, with bars, in the positive axis are non-stoichiometric toward A; those in the negative axis are non-stoichiometric toward B, and those in both axes are stoichiometric. Co_2NiO_4 is tagged with the star, as data presented here is of zero charge state at the top of the valance band (VBM), because of difficulty in calculating δH of a charged state due to its metallic band structure.

known as self doping. In fact, in the majority of the spinels, this process is the main source of charge carriers.[18]

Experimentally, site occupancy can be measured by several techniques, such as anomalous x-ray diffraction (AXRD), extended x-ray absorption fine structure (EXAFS), neutron diffraction, Mössbauer spectroscopy, and, less frequently, x-ray emission spectroscopy (XES). For example, EXAFS and Mössbauer spectroscopy have been used to confirm that Co_2NiO_4 is an inverse spinel.[19] Similarly, Eba and Sakurai[20] used XES to show that Mn_2LiO_4, Mn_2ZnO_4, Mn_2CrO_4, Cr_2MnO_4, and Ga_2MnO_4 are normal, and Mn_2CoO_4 is an inverse spinel, whereas neutron diffraction was used to establish that In_2CdO_4 (Ref. 21) and Mn_2CuO_4 (Ref. 22) are disordered inverse spinels with different degrees of inversion. Here we used AXRD[23] to measure the site occupancy in Co_2ZnO_4. In this technique, the scattering strength of one element is changed by varying the x-ray energy near the element absorption edge, and several diffraction peaks are measured at the various energies. This yields site-specific occupancies.[24] Note that conventional XRD is unable to determine the site occupancy when atoms involved have similar atomic number (e.g., Zn and Co).

Nonstoichiometry and phase-boundaries in the x-T phase diagram. A ternary two-cation oxide (A_2BO_4) appears in an x-T phase diagram in equilibrium with binary A_lO_n and B_mO_n competing phases with stoichiometry (l,n) and (m,n). The site occupancy in a compound (A_2BO_4) under A-rich and B-rich conditions determines its phase boundary. The phase boundary combined with the identity of competing phases can be used to construct the x-T phase diagram. This diagram differs from conventional phase diagrams found in textbooks and compilations[10] in that it lacks information about melting and eutectic points.

In this paper, we present the calculated (a) nonstoichiometry, (b) site occupancies, and (c) phase boundaries of two prototypical normal spinels, Co_2ZnO_4 and Rh_2ZnO_4, along with the experimental phase boundaries determined via XRD and Rietveld refinement and site occupancies determined via AXRD in the case of Co_2ZnO_4. With this we show that Co_2ZnO_4 is naturally Co rich, whereas Rh_2ZnO_4 is only slightly Zn rich at higher temperatures. The phase stability region in these spinels is dictated by their heats of substitution of antisite defects. Calculated heats of substitution for a number of spinels reveal that $\Delta H(A_{T_d})$ is generally smaller than $\Delta H(B_{O_h})$ if the A-rich competing phase is isostructural with the A_2BO_4 host, while the B-rich competing phase is not. We then use this argument to explain the nonstoichiometry and wide solid solutions existing in other spinel oxides.

II. THEORY OF CATION NONSTOICHIOMETRY IN SPINELS

Nonstoichiometry in a normal spinel, A_2BO_4, is the difference in the number of antisite A and B species:

$$\begin{aligned}\Delta B &= N\left(B_{O_h}\right) - N\left(A_{T_d}\right),\\ \Delta A &= N\left(A_{T_d}\right) - N\left(B_{O_h}\right),\end{aligned} \tag{1}$$

with the number of A atoms substituting on T_d sites, and the number of B atoms substituting on O_h sites being

$$\begin{aligned}N\left(A_{T_d}\right) &= N_{T_d}\exp\left(\frac{-\Delta H\left(A_{T_d}\right)}{kT}\right),\\ N\left(B_{O_h}\right) &= N_{O_h}\exp\left(\frac{-\Delta H\left(B_{O_h}\right)}{kT}\right),\end{aligned} \tag{2}$$

where N_{T_d}, N_{O_h}, q, k, and T represent the number of tetrahedral sites, number of octahedral sites, charge state, Boltzmann constant, and temperature, respectively, and ΔH are corresponding enthalpies of substitution. These expressions are derived from the minimization of the Gibbs free energy of a defective cell with respect to the concentration of defects assuming ΔH is independent of defect concentration and only the configurational entropy resulting from different ways of arranging defects among the available numbers of sites is taken into account.

Each enthalpy of substitution ($\Delta H^{(q)}$) of A_{T_d} and B_{O_h}, a function of charge (q), chemical potential of A (μ_A) and B (μ_B) and Fermi energy (E_F), is calculated by considering a system to be in thermodynamic equilibrium with a reservoir, with which one exchanges the atoms and charges in the case of charged defects:

$$\begin{aligned}\Delta H^{(q)}\left(B_{O_h}\right) &= \left[E_D\left(B_{T_d}\right) - E_H\right] + (\mu_A - \mu_B) + q(E_v + E_F),\\ \Delta H^{(q)}\left(A_{T_d}\right) &= \left[E_D\left(A_{T_d}\right) - E_H\right] + (\mu_B - \mu_A) + q(E_v + E_F),\end{aligned} \tag{3}$$

where E_H and E_D are the energy of the defect-free host (H) and defect (D)-containing host. The chemical potentials $\mu_A = \mu_A^{el} + \Delta\mu_A$ and $\mu_B = \mu_B^{el} + \Delta\mu_B$ are defined with respect to elemental phases. The chemical potentials ($\Delta\mu$) are fixed by the thermodynamic conditions such that A_2BO_4 exists without decomposing into competing elemental A, B, and O, binaries A_lO_n and B_mO_n and other ternaries $A_lB_mO_n$ phases, that is, $2\Delta\mu_A + \Delta\mu_B + 4\Delta\mu_O = \Delta H_f(A_2BO_4)$, where ΔH_f is the formation (f) enthalpy of the compound. These conditions limit the range of accessible chemical potentials for a compound, which is further reduced by growth conditions. For example, a particular choice of a temperature and pressure (converted to an oxygen chemical potential using the ideal gas law) results in a reduction of the accessible chemical potential range (shaded in yellow) to a portion of dotted line in the shaded area as shown in Figs. 4 and 5.

The remaining parameters needed to determine antisite occupancy $N(A_{T_d})$ and $N(B_{O_h})$ are E_F and T. E_F itself depends upon number of charge carriers, which, in turn, depends upon the ionized $N(A_{T_d})$ and $N(B_{O_h})$. We then self-consistently determine $N(A_{T_d})$, $N(B_{O_h})$, the number of carriers, and E_F by requiring overall charge neutrality of a system.[25]

Nonstoichiometry results from excess of one of two antisite occupancies. The excess of A is when the enthalpies of substitution show

$$\Delta H\left(A_{T_d}\right) < \Delta H\left(B_{O_h}\right). \tag{4}$$

However, $\Delta H(A_{T_d})$ depends on the energy difference between the defect and host cell, as well as the chemical energy $\Delta\mu_A$ and $\Delta\mu_B$ of the involved elements A and B, which

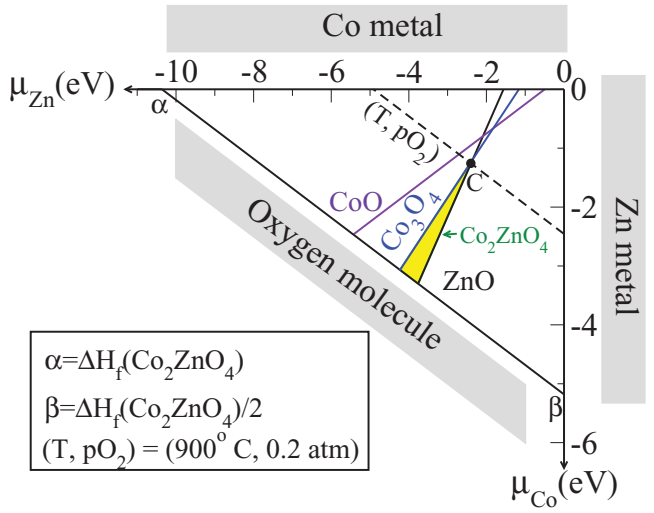

FIG. 4. (Color online) Chemical potential stability plot of Co_2ZnO_4. The area shaded in yellow represents the range of accessible chemical potentials under thermodynamical equilibrium, and the line in shaded area represents the specific growth conditions. The Zn- and Co-rich conditions are defined by Co_2ZnO_4/ZnO and Co_2ZnO_4/Co_3O_4 equilibrium lines. The maximum of Zn-rich and Co-rich chemical potentials coincides with point C. Other possible competing phases, such as CoO and CoO_2 require Co-rich/Zn-poor conditions and Zn_2CoO_4 requires Zn-rich/Co-poor conditions that are far away from accessible chemical potentials of Co_2ZnO_4.

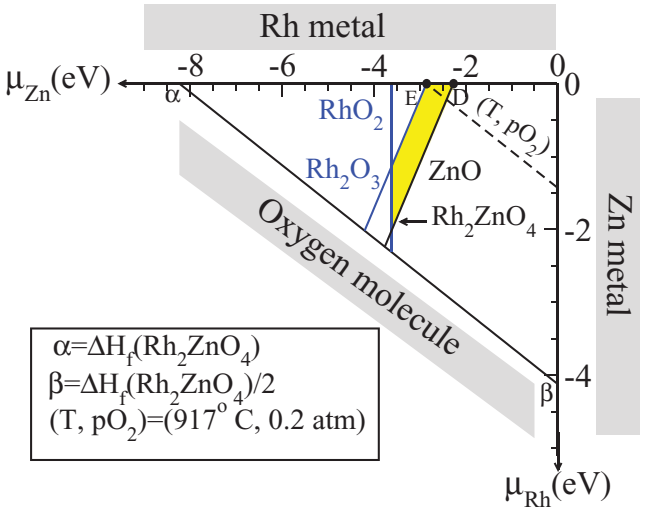

FIG. 5. (Color online) Chemical potential stability plot of Rh_2ZnO_4. The area shaded in yellow represents the range of accessible chemical potentials under thermodynamical equilibrium, and the line in the shaded area represents the specific growth conditions. The Rh-rich and Zn-rich conditions are defined by Rh_2ZnO_4/Rh_2O_3 and Rh_2ZnO_4/ZnO equilibrium lines. The maximum Zn- and Rh-rich conditions are indicated by point D and point E, respectively. Other possible competing phases, such as Rh_3O_4, require Rh-rich/Zn-poor conditions, and Zn_2RhO_4 requires Zn-rich/Rh-poor conditions that are far away from accessible chemical potentials of the Rh_2ZnO_4. Points D and E define maximally accessible Zn-rich conditions, and one of the maximally accessible Rh-rich chemical potential conditions.

depends upon the competing phases, as they are bounded by their heats of formation. Competing phases can be thought of as the reservoir, with which one exchanges atoms during antisite creation. So if the reservoir and system are structurally and chemically similar, then the enthalpy of formation would be naturally low, leading to higher antisite occupancies and nonstoichiometry.

III. COMPUTATIONAL DETAILS

We used projector augmented-wave (PAW)[26] Perdew-Burke-Ernzerhof (PBE)[27] pseudopotential within the density functional theory (DFT) band structure approach as implemented in VASP code.[28,29] A soft pseudopotential for oxygen with the kinetic energy cutoff of 300 eV is chosen for ionic relaxation, whereas an energy cutoff up to 450 is used for the volume relaxation. Exchange and correlation effects beyond Generalized gradient approximation (GGA) are treated in rotationally invariant GGA + U formalism,[30] with U determined in such a way that it correctly reproduces relative stability of competing binaries such as Co_3O_4 and CoO and Rh_2O_3 and RhO_2 as described by Lany *et al.*[2] The values of U determined in such a way for Co and Rh were 3.0 and 3.3 eV, respectively.

Defect calculation was performed in a 56-atom cubic cell with $2 \times 2 \times 2$ Monkhorst-Pack[31] k points. Energy of formation was corrected for the image charges, potential alignment and band filling effect as described in detail by Lany and Zunger.[32] The band gap was corrected using *a posteriori* shift of the conduction band minimum.[32] The dielectric constants necessary in the image charge correction were calculated using density functional perturbation approach[33] as implemented in VASP.

IV. EXPERIMENT

A. Sample preparation

Bulk polycrystalline equilibrium samples were synthesized via an aqueous synthesis route (decomposition of nitrates) to prepare samples in the low-temperature ZnO-Co_3O_4 system, since, unlike conventional solid-state processing, this approach enables cation mixing at the atomic level at low temperatures in a reasonable time frame. Weight-loss analysis of cobalt nitrate hexahydrate, 99.999%, and zinc nitrate hexahydrate, 99.998% (both Alfa Aesar, Ward Hill, MA), upon heating to remove water and nitrogen was performed in pre-dried crucibles to determine the exact water content in the starting nitrates. Stoichiometric amounts of the Co and Zn nitrate hydrates were then added to deionized water to give cation ratios, Co/(Zn + Co), of 0.08, 0.12, 0.16, 0.633, 0.667, 0.70, 0.73, 0.767, 0.80, 0.833, 0.85, 0.90, 0.95, and 1. The nitrate solutions were stirred continuously at 40 °C–50 °C to mix the cations and evaporate most of the water. Then the concentrated solutions/gels were heated to 390 °C in a box furnace in a fume hood to burn out residual water and nitrogen oxides, resulting in the formation of cobalt zinc oxide powders. Powders were then ground in a mortar and pestle and pressed uniaxially at 125 MPa into pellets and sintered in air for 60 h at various temperatures (650 °C and 800 °C). [Powders were also prepared at 500 °C, and those with a composition

of $Co/(Zn + Co) = 0.633$ were additionally prepared at 390 °C, 450 °C, and 575 °C.] During sintering the pellets were surrounded by sacrificial powder of the same composition and nested inside three concentric crucibles, in order to minimize both contamination and cation volatilization. The extended sintering time, followed by quenching in air, was chosen to promote equilibration of the samples at the temperatures of interest. (For the lowest-temperature samples, XRD was performed after different sintering times to ensure that the phase composition of the sample did not evolve with further sintering.) Cation ratios were confirmed for selected samples using wavelength-dispersive x-ray fluorescence with a Bruker S4 Pioneer spectrometer (Bruker AXS Inc., Madison, WI).

For the ZnO-Rh_2O_3 system, three bulk polycrystalline biphasic samples of Zn-rich compositions relative to Rh_2ZnO_4 were fabricated via conventional solid-state synthesis. Starting powders of ZnO (Alfa Aesar) of purity >99.99% and Rh_2O_3 (Strem Chemicals Inc., Newburyport, MA, USA, and Sigma-Aldrich, St. Louis, MO, USA) of purity >99.8% were dried overnight and ground together with mortar and pestle. The target compositions, in terms of fractional rhodium content [Rh/(Zn + Rh)] were 0.62, 0.60, and 0.57. Pellets of 0.5-inch diameter were pressed at approximately 130 MPa.

As with the Zn-Co-O system, the pellets were surrounded with sacrificial powder and placed in three nested aluminum oxide crucibles. The samples were sintered in air at 975 °C for 20 h and slow cooled to room temperature at 5 °C/min. They were then ground and pressed once more and given the same heat treatment. For both systems, the sample surfaces were lightly ground prior to characterization by XRD and AXRD in order to mitigate any surface effects. The achieved pellet densities were consistently approximately 50% of the theoretical density, based on mass and dimensional measurements.

B. Site occupancy measurements

Site-specific cation occupancies are obtained from K-edge AXRD obtained on the powder diffraction beam line 2-1 at the Stanford Synchrotron Radiation Light source (SSRL). AXRD selectively probes the cations populating the crystallographically inequivalent octahedral and tetrahedral sites of the spinel crystal structure. The (222) reflection of the spinel structure is sensitive to only the octahedral sites, while the (422) peak depends solely on the tetrahedral site occupancy.[24] This allows relatively straightforward separation of the octahedral and tetrahedral site occupancies. Data were obtained for both (422) and (222) peaks at the Co and Zn K edges. Modeling of the AXRD spectra provided the cation inversion.[34]

C. Phase boundary determination by Rietveld refinement (lever rule, intercept method/disappearing phase method)

Phase identification and composition were determined by room-temperature XRD. For the ZnO-Co_3O_4 system, a Scintag XDS2000 diffractometer (Scintag Inc., Cupertino, CA), with Cu $K\alpha$ radiation, a step size of 0.02°, and a dwell time of 1 s, was used to collect scans in the 2θ range of 25°–80°. For the ZnO-Rh_2O_3 system, XRD was carried out on a Rigaku diffractometer (Rigaku, The Woodlands, TX, USA) with a Cu $K\alpha$ source and a Ni filter; these data were collected from $2\theta = 10°$–80°, with a step size of 0.05° and a dwell time of 1 s. The relevant powder diffraction files used for pattern matching were PDF No. 00-041-0134 for Rh_2ZnO_4 and PDF No. 01-070-8072 for ZnO. For both systems, structureless Rietveld refinement was conducted on the resulting intensity vs 2θ scans using JADE 8 and JADE 9 software packages, in order to determine the weight percent of each phase present. Two complementary methods were then applied to determine phase boundaries at the quench temperatures. (a) Using the Lever rule, spinel phase boundary compositions were determined from the phase content of each individual sample. In the case of the ZnO-Co_3O_4 system, the phase boundary for Co solubility in ZnO at different temperatures was determined first (using the "intercept method"[35]) in order to enable the calculation of the spinel phase boundary from the remaining data. The "intercept/disappearing phase method" was applied when data for a number of compositions at a given temperature were available. The weight percent of the nonspinel phase (wurtzite) was plotted as a function of nominal wurtzite weight fraction (based on overall sample composition) for that temperature, and the composition at which the second-phase content became zero (the composition-axis intercept) was assigned as the phase boundary composition. Applying both of these methods provides more reliability in phase boundary determination than using Rietveld refinement of a single sample alone.

V. RESULTS

A. Site occupancy: Experiment and theory

Co_2ZnO_4 and Rh_2ZnO_4 are predicted to be normal spinels at $T = 0$ based on comparison of DFT total energy of a normal and various inverse configurations[36] as well as various empirical models.[8,37] This means that, at the zero temperature, there are no antisite defects. However, at finite temperature antisite defects start to appear. The number of antisite defects depends on the enthalpy of substitution and temperature. The calculated enthalpy of substitution of a dominant defect is presented in Fig. 3 for a number of spinels at self-consistently determined E_F and maximum A-rich chemical potential to correlate with the maximum (possible) A nonstoichiometry and B-rich chemical potential to correlate with (possible) B nonstoichiometry. Dominant charge states for Ga_2CdO_4, Al_2MgO_4, Ga_2ZnO_4, and Ga_2MnO_4 are 1− for B_{O_h} and 1+ for A_{T_d}, whereas those for Co_2ZnO_4, Co_2NiO_4, and Rh_2ZnO_4 are zero for A_{T_d} and 1− for B_{O_h}, and those of Cr_2MnO_4 are neutral for both A_{T_d} and B_{O_h}.

Now, focusing on the case Co_2ZnO_4, we found that the calculated ΔH (Zn_{O_h}) in Co_2ZnO_4 is much higher than ΔH (Co_{T_d}) so that $N(Zn_{O_h})$ is much smaller than $N(Co_{T_d})$ in both Zn-rich and Co-rich conditions, as shown in Fig. 6 for all temperatures at which the compound is stable. $N(Zn_{O_h})$ in Co_2ZnO_4 is negligible, so we predict the compound to remain normal even at higher temperatures. Furthermore, ΔH (Co_{T_d}) at the Co-rich limit is practically zero leading $N(Co_{T_d})$ to be more than 50% of T_d sites.

We have performed AXRD measurements on samples of $Co_{2.3}Zn_{0.7}O_4$ and $Co_{2.7}Zn_{0.3}O_4$ powders prepared as previously mentioned at 800 °C. Within the detection limit of these experiments (approximately 1%), we find that all of the O_h sites

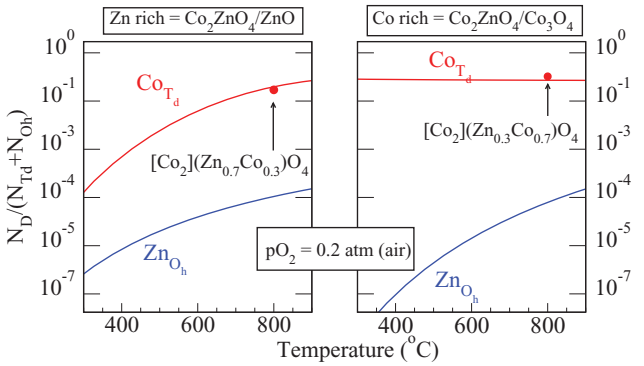

FIG. 6. (Color online) Calculated fraction of antisite defects in Co_2ZnO_4 under Zn-rich (left) and Co-rich (right) conditions compared with those (solid circle) measured using AXRD in bulk ceramic sintered samples.

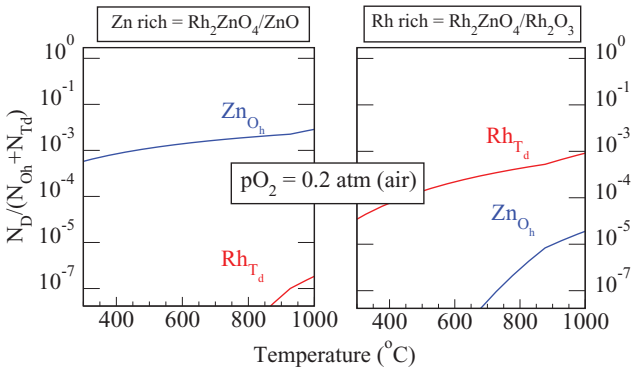

FIG. 7. (Color online) Calculated fraction of antisite defects in Rh_2ZnO_4 under Zn-rich (left) and Rh-rich (right) conditions.

are occupied by Co. The T_d sites are comprised of all of the Zn and the excess Co (0.3 for the $Co_{2.3}Zn_{0.7}O_4$ sample and 0.7 for the $Co_{2.7}Zn_{0.3}O_4$ sample), thus making these samples normal spinels. Figure 6 shows a comparison of the experimentally determined site occupancy to the defect calculations for 800 °C in air. There is excellent quantitative agreement for the Co occupancy on T_d sites between the measurement and the calculation. A stoichiometry of $Co_{2.3}Zn_{0.7}O_4$ is calculated at the Co_2ZnO_4/ZnO boundary at 800 °C, similar to that of the $Co_{2.3}Zn_{0.7}O_4$ sample, while a stoichiometry of $Co_{2.5}Zn_{0.5}O_4$ is calculated at the Co_2ZnO_4/Co_3O_4 boundary at 800 °C, similar to the $Co_{2.7}Zn_{0.3}O_4$ sample. Thus, slight deviations between the experimental and the calculated site occupancies in Fig. 6 result because the stoichiometries are not exactly the same. Finally, we are unable to experimentally produce a single-phase spinel sample with a Zn:Co ratio greater than 1:2. This is consistent with the calculations that show $N(Co_{T_d})$ is much higher than $N(Zn_{O_h})$, even at the Zn-rich limit.

We next compare our site occupancy results with the existing literature results. Site occupancy measurements in the existing literature are reported for samples grown via thermodynamic equilibrium methods and nonequilibrium methods. The EXAFS measurements by Porta *et al.*[38] on samples prepared via coprecipitation found Zn exclusively in the T_d site. However, neutron diffraction measurements by Krezhov *et al.*[39] on a sample prepared via a thermal decomposition show an inversion of 0.2, possibly due to the precursor yielding a higher degree of inversion indicating a nonequilibrium distribution of cations. Indeed, samples grown from nonequilibrium methods tend to show a certain degree of inversion. For example, samples prepared by CVD[40] and sputtering[41] show some Zn in O_h sites, whereas Dekkers *et al.*[42] have inferred the presence of Co in T_d sites in a polycrystalline Co_2ZnO_4 thin film, to explain their optical data. Similarly, Perkins *et al.*[41] found a higher degree of inversion in sputtered thin film samples compared to samples prepared via thermal equilibrium synthesis.

In the case of Rh_2ZnO_4, the calculated heat of substitution plotted in Fig. 3 and site occupancy plotted in Fig. 7 show the following: (a) Both ΔH (Zn_{O_h}) and ΔH (Rh_{T_d}) are high, so that $N(Zn_{O_h})$ and $N(Rh_{T_d})$ are small, and thus Zn and Rh are effectively confined to T_d and O_h sites, respectively, indicating that the compound is also a normal spinel even at higher temperature; and (b) the enthalpy of substitution and hence antisite occupancy is dictated by chemical potential conditions, that is, at the Zn-rich limit ΔH (Rh_{T_d}) is higher than ΔH (Zn_{O_h}); hence, $N(Zn_{O_h})$ exceeds $N(Rh_{T_d})$, while at the Rh-rich limit ΔH (Zn_{O_h}) is higher than ΔH (Rh_{T_d}) and hence $N(Rh_{T_d})$ exceeds $N(Zn_{O_h})$.

Co_2ZnO_4 and Rh_2ZnO_4, both normal spinels, differ from each other in terms of the possible number of antisite defects. In Co_2ZnO_4, even under the Zn-rich conditions $N(Co_{T_d})$ exceeds $N(Zn_{O_h})$, whereas in Rh_2ZnO_4, $N(Zn_{O_h})$ exceeds $N(Rh_{T_d})$. However, for the *A*-rich limit, $N(A_{T_d})$ are higher than $N(B_{O_h})$ for both compounds. This different behavior affects the phase boundary and nonstoichiometry in these two compounds.

B. Nonstoichiometry: Experiment and theory

The site occupancy measurements and calculations shown in Figs. 6 and 7 under *A*- and *B*-rich conditions can be rearranged to calculate the phase boundary as a function of the temperature. In what follows, we present the phase boundary of Co_3O_4 vs Co_2ZnO_4 and address the issue of a solid solution between them.

1. Co_2ZnO_4: Case of a solid solution with Co_3O_4 (Co_2CoO_4)

In Fig. 8 we plot the stability region of Co_2ZnO_4 ($Co_{2+x}Zn_{1-x}O_4$) and Zn-substituted Co_3O_4 ($Co_{3-y}Zn_yO_4$) as function of the temperature. In case of Co_2ZnO_4, not only the Co-rich phase boundary, as in case (a) of Fig. 1, but also the Zn-rich phase boundary deviate toward the high valent cation Co. As can be seen in Fig. 4, the immediate Co-rich competing phase of Co_2ZnO_4 is Co_3O_4. Since both of these systems are spinels, it is interesting to investigate how the Zn-rich phase boundary, that is, Co_3O_4/Co_2ZnO_4 of Zn-substituted Co_3O_4, evolves with temperature. We found that this boundary deviates toward the lower valent cation Zn and overlaps with the Co-rich/Zn-poor boundary of Co_2ZnO_4 even at room temperature, forming a solid solution, as suggested by Petrov *et al.*[43] The stability region of this solid solution is bounded on the Zn-rich side by the Zn-rich boundary of Co_2ZnO_4 and pure Co_3O_4 on the Co-rich side.

As was mentioned in Sec. IV C, a number of samples of different compositions and synthesis temperatures were measured by XRD and analyzed by Rietveld refinement in

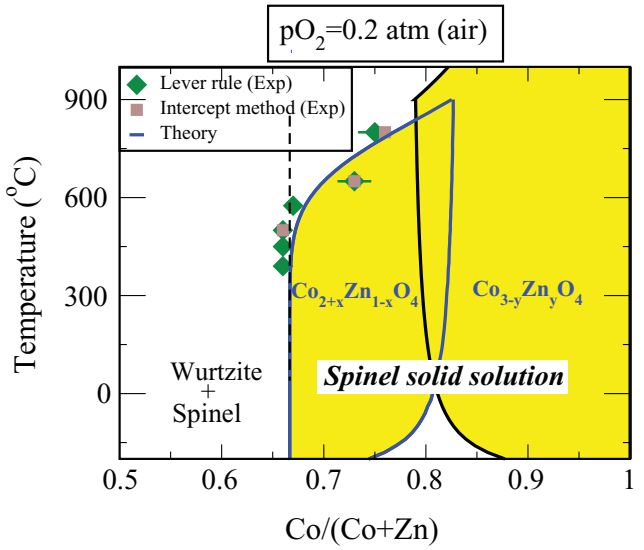

FIG. 8. (Color online) Calculated stability region of $Co_{2+x}Zn_{1-x}O_4$ within blue boundary and $Co_{3-y}Zn_yO_4$ in the black boundary. Two stability regions overlaps one another, indicating that no miscibility gap between the two spinels even at room temperature and that they form a solid solution. Green diamonds and brown squares indicate the experimental phase boundary obtained by level rule and the intercept method, respectively. (At 650 °C the Lever rule and intercept method points overlap.)

order to determine the phase boundaries of the spinel regions in Zn-Co-O and Zn-Rh-O. From the weight percent of the second phase in each case, determined by Rietveld refinement, two approaches (Lever rule and intercept method/disappearing phase method) were then used to determine the phase boundary composition for a given temperature. Table III (see the Appendix) summarizes these resulting phase boundary compositions from each method. For Zn-Co-O it can be seen that, for the higher temperatures, the spinel phase boundary lies on the Zn-poor/Co-rich side of the nominal Co_2ZnO_4 composition of $Co/(Zn + Co) = 0.667$. This means that samples prepared with an overall Zn-rich composition contain two phases: a cobalt-rich spinel and wurtzite (cobalt-substituted ZnO). Excellent agreement was found between the average Lever rule and intercept method phase boundaries.

The experimental results strongly support the calculated phase boundary of the spinel phase, as can be seen in Fig. 8. Both theory and experiment show that the spinel phase exists only for Zn-poor compositions above ≈500 °C, consistent with the Co_3O_4-ZnO phase diagram of Robin *et al.*[44] We calculated the Co_2ZnO_4 spinel phase to be unstable above 900 °C in agreement with the diagram by Robin *et al.* We calculated the Co_3O_4 spinel phase decomposes to CoO at 1200 °C in agreement with the measured enthalpy of formation.[45] Decomposition temperature in the literature, however, is suggested to be 900 °C.[44,46–52] Both of these values lie with in error bar of our calculations.

2. Rh_2ZnO_4: Case of a line compound

Figure 9 shows the calculated Rh_2ZnO_4 phase boundaries. Notice that the Zn-rich and Rh-rich boundaries lie virtually on top of each other, indicating that Rh_2ZnO_4 is, to a large extent,

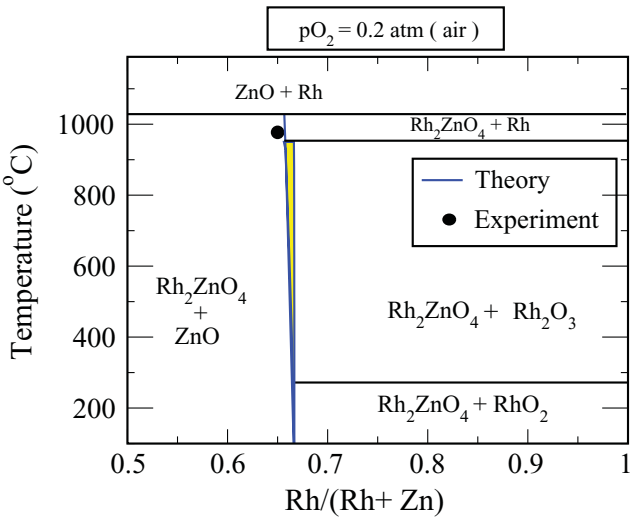

FIG. 9. (Color online) Theoretically calculated phase diagram for Rh_2ZnO_4. The experimental phase boundary determined by Rietveld refinement for the bulk ceramic sample is shown as a black solid circle.

a line compound. It is only at high temperature that the Zn-rich boundary starts separating from the Rh-rich boundary making the compound able to incorporate Zn excess.

The results of the Rietveld refinement for phase boundary determination are also listed at the bottom of Table III (see the Appendix). As shown in the table, the phase boundaries calculated by the lever rule are in excellent agreement with each other. Using these data points in a disappearing phase analysis (intercept method), the phase boundary is calculated to occur at a composition of $Rh/(Zn + Rh) = 0.65$, which is consistent with the lever rule method. These experimental values are also in excellent agreement with the theoretically predicted phase boundary of the Zn-rich compound under the same synthesis conditions: $Rh/(Zn + Rh) = 0.658$.

Only two earlier measurements on Rh_2ZnO_4 are available. The EDX and XPS measurement by Mizoguchi *et al.*[53] shows the Zn/Rh ratio to be 0.5 for both polycrystalline thin films and pressed pellet samples prepared by conventional solid-state reaction. Further, Banerjee *et al.*[54] also concluded that Rh_2ZnO_4 is a stoichiometric compound based on the phase diagram constructed from an emf measurement in an oxide solid-state electrochemical cell. Our results are in good agreement with these prior studies, that is, that Rh_2ZnO_4, to a large extent, is a stoichiometric compound.

VI. *A* AND *B* NONSTOICHIOMETRY CORRELATED WITH EXISTENCE OR ABSENCE OF COMPETING ISOSTRUCTURAL PHASES

The significant deviation of Co_2ZnO_4 toward Co can be correlated with the existence of the isostructural competing phase Co_3O_4. $\Delta H(A_{T_d})$ is smaller than $\Delta H(B_{O_h})$, if the *A*-rich competing phase is isostructural with the A_2BO_4 host, whereas the *B*-rich competing phase is not. Thus, from knowledge of the competing phases of a compound, one can guess which of two antisite substitutions is favored. Figure 3 gives the calculated enthalpies of substitution and Table I gives known competing phases. For example, we see

TABLE I. Table shows different A_2BO_4 spinels, corresponding A-rich and B-rich phases, and predicted nonstoichiometry deviation. Structure of competing phases that are similar to the host spinel are given in the parentheses. Hausmannite (H) has a distorted spinel structure. Thus, in the table, if structure of only one competing phase is given, such spinel would deviate toward that cation, whereas if both competing phases have spinel-like structure, the spinel phase would be nonstoichiometric toward the competing phase that is more similar to spinel than the other. In the final column, – means not known.

Compound(S)	A-rich phase	B-rich phase	Predicted nonstoichiometry	Observed nonstoichiometry
Al_2MgO_4	Al_2O_3	MgO	Neither	Both
Ga_2CdO_4	Ga_2O_3	CdO	Neither	Ga
Mg_2TiO_4	MgO	TiO_2	Neither	Neither
Cr_2MnO_4	Mn_3O_4 (H)	Cr_2O_3	Mn	Mn
Co_2ZnO_4	Co_3O_4 (S)	ZnO	Co	Co
Rh_2ZnO_4	Rh_2O_3	ZnO	Neither	Slightly Zn-rich
Co_2NiO_4	Co_3O_4 (S)	NiO	Co	Co
Cr_2MgO_4	Cr_2O_3	MgO	Neither	Mg
Cr_2FeO_4	Cr_2O_3	Fe_3O_4(S)	Fe	Fe
Fe_2CrO_4	Fe_3O_4 (S)	Cr_2FeO_4 (S)	Fe	Fe
Al_2FeO_4	Al_2O_3	Fe_3O_4(S)	Fe	Mostly Fe
Mn_2CoO_4	Mn_3O_4 (H)	Co_2MnO_4 (S)	Both	Both
Mn_2FeO_4	Mn_3O_4 (H)	Fe_2MnO_4 (S)	Both	Both
Mn_2CuO_4	Mn_3O_4 (H)	CuO	Mn	Both
Ga_2ZnO_4	Ga_2O_3	ZnO	Ga	–
Ga_2MnO_4	Ga_2O_3	Mn_3O_4(H)	Mn	–
Mn_2GeO_4	Mn_3O_4 (H)	GeO_2	Mn	–
Mn_2SiO_4	Mn_3O_4 (H)	SiO_2	Mn	–
Mn_2SnO_4	Mn_3O_4 (H)	SnO_2	Mn	–
Mn_2NiO_4	Mn_3O_4 (H)	NiO	Mn	–
Fe_2CuO_4	Fe_3O_4 (H)	Cu_2O	Fe	–
Fe_2AlO_4	Fe_3O_4 (S)	Al_2O_3	Both	–
Al_2FeO_4	Fe_2AlO_4 (S)	Al_2O_3	Both	–
Mn_2CrO_4	Mn_3O_4 (H)	Cr_2MnO_4 (S)	Both	–
Co_2MnO_4	Mn_2CoO_4 (S)	Co_3O_4 (S)	Both	–
Fe_2MnO_4	Fe_3O_4 (S)	Mn_2FeO_4 (S)	Both	–
Mn_2AlO_4	Mn_3O_4 (H)	Al_2O_3	Mn	–
Al_2MnO_4	Mn_3O_4 (H)	Mn_2AlO_4(S)	Mn	–
Fe_2CoO_4	Fe_3O_4 (S)	Co_2FeO_4(S)	Both	

that ΔH (Co_{T_d}) is smaller than ΔH (Zn_{O_h}) in Co_2ZnO_4, consistent with Co_3O_4 (Co_2CoO_4) being isostructural but not ZnO. The same is true for the other materials such as Cr_2MnO_4, Ga_2MnO_4, Cr_2FeO_4, and Fe_2CuO_4, where isostructural competing phases are Mn_2MnO_4 (hausmannite) and Fe_2FeO_4 (spinel), indicating that the phase stability regions of these materials will deviate toward the respective isostructural competing phases. However, the degree of deviation depends not only on $\Delta H(A_{T_d})$, but also on $\Delta H(B_{O_h})$. For the pronounced nonstoichiometry toward A, one requires a small $\Delta H(A_{T_d})$ and relatively larger $\Delta H(B_{O_h})$ and for pronounced nonstoichiometry toward B, one requires a small $\Delta H(B_{O_h})$ and relatively larger $\Delta H(A_{T_d})$ at equilibrium E_F. These conditions are satisfied by compounds such as Co_2ZnO_4,

TABLE II. Inter-transition-metal oxide compounds with spinel or similar structure between elements with multiple oxidation state. The compounds bounded by vertical lines shows a tendency to form a solid solution.

System	←A/B rich→					
Cr-Mn-O	Cr_2O_3		Cr_2MnO_4	Mn_2CrO_4	Mn_3O_4	Mn_2O_3
Cr-Fe-O	Cr_2O_3		Cr_2FeO_4	Fe_2CrO_4	Fe_3O_4	
Cr-Co-O	Cr_2O_3		Cr_2CoO_4	Co_2CrO_4	Co_3O_4	CoO
Fe-Al-O	Fe_2O_3	Fe_3O_4	Fe_2AlO_4	Al_2FeO_4	γ-Al_2O_3	β-Al_2O_3
Fe-Cr-O	Fe_2O_3	Fe_3O_4	Fe_2CrO_4	Cr_2FeO_4		Cr_2O_3
Fe-Mn-O	Fe_2O_3	Fe_3O_4	Fe_2MnO_4	Mn_2FeO_4	Mn_3O_4	M_2O_3
Fe-Co-O	Fe_2O_3	Fe_3O_4	Fe_2CoO_4	Co_2FeO_4	Co_3O_4	CoO
Mn-Cr-O	Mn_2O_3	Mn_3O_4	Mn_2CrO_4	$MnCr_2O_4$		Cr_2O_3
Mn-Co-O	Mn_2O_3	Mn_3O_4	Mn_2CoO_4	$MnCo_2O_4$	Co_3O_4	CoO

where $\Delta H(A_{T_d}) \approx 0.0$ eV and $\Delta H(B_{O_h}) = 0.86$ eV so the system is B deficient, by Cr_2MnO_4, where $\Delta H(A_{T_d}) = 1.98$ eV and $\Delta H(B_{O_h}) = 0.73$ eV so the system is A deficient. However, in compounds such as Al_2MgO_4 [$\Delta H(A_{T_d}) = 0.40$ eV; $\Delta H(B_{O_h}) = 0.55$ eV] and Ga_2CdO_4 [$\Delta H(A_{T_d}) = 0.28$ eV; $\Delta H(B_{O_h}) = 0.44$ eV], both $\Delta H(A_{T_d})$ and $\Delta H(B_{O_h})$ are small and comparable; hence, they form nearly equal but large numbers of antisites defects A_{T_d} and B_{O_h}. This means that these compounds would prefer inversion ($\lambda > 0$) with nearly perfect stoichiometry (A:$B \approx 2$:1) at higher temperatures. Experimentally, however, it is known that Al_2MgO_4 is either Al or Mg rich,[55] and Ga_2CdO_4 is Cd rich[56] at higher temperature. Defective spinels (spinels with the two cation vacancies), γ-Al_2O_3,[57,58] appear as a penultimate Al-rich competing phase of Al_2MgO_4. Similarly, γ-Ga_2O_3[59,60] appears as a penultimate Ga-rich competing phase of Ga_2CdO_4. The energy difference between the defective spinel phase and the ground-state phase is ≈40 meV/atom in both Al_2O_3 and Ga_2O_3. Theoretically, even if when such phases are considered as hypothetical competing phases of the spinel, we still find these compounds to prefer inversion over nonstoichiometry. The reason for this disagreement between theory and experimental fact in these compounds is unclear at the present.

In Table II, we have tabulated a number of spinels along with the expected nonstoichiometry direction based on the presence or absence of isostructural competing phases along with the observed nonstoichiometry. From this table, one can see that the presence or absence of a isostructural competing phase is often (but not always) sufficient to indicate the direction of nonstoichiometry. Furthermore, the existence of solid solutions[61] between mixed transition-metal oxides (involving both transition-metal elements and transition-metal and main-group elements) can also be inferred from this argument alone. For example, possible A_2BO_4 stoichiometries between Fe and Mn oxides are Fe_3O_4, Fe_2MnO_4, Mn_2FeO_4, and Mn_3O_4, in which Fe_2MnO_4 and Mn_2FeO_4 deviate toward either direction and possibly form a solid solution between each other and with end members Fe_3O_4 and Mn_3O_4 at higher temperatures. Such possibilities exist for a number of other combinations of mixed transition-metal compounds, as tabulated in Table II.

VII. CONCLUSION

We investigated the nonstoichiometry and phase boundaries in typical spinels Co_2ZnO_4 and Rh_2ZnO_4 both experimentally and theoretically using variety of techniques and found that Co_2ZnO_4 is nonstoichiometric toward Co(A), whereas Rh_2ZnO_4 is only slightly nonstoichiometric toward Zn (B) and both of these compounds remain normal even at high temperatures. In Co_2ZnO_4, small ΔH (Co_{T_d}) compared to ΔH (Zn_{O_h}) is the main cause of nonstoichiometry toward Co, whereas in Rh_2ZnO_4 both antisite defects have relatively high formation energies and nonstoichiometry is very small toward Zn. A simple correlation that can be drawn from these opposite trends of nonstoichiometry, that is, if a competing phase A_lO_n or B_mO_n is isostructural having similar bond length with a compound A_2BO_4, the compound will be nonstoichiometric in that direction. This observation is sufficient to qualitatively predict the nonstoichiometry in many other spinel systems involving both main-group and transition-metal compounds.

ACKNOWLEDGMENTS

This work was supported through the Center for Inverse Design, an Energy Frontier Research Center funded by the US Department of Energy, Office of Science, Office of Basic Energy Sciences and made use of the J. B. Cohen X-Ray Diffraction Facility supported by the MRSEC program of the National Science Foundation (Grant No. DMR-0520513) at the Materials Research Center of Northwestern University. Portions of this research were carried out at the Stanford Synchrotron Radiation Lightsource, a national user facility operated by Stanford University on behalf of the US Department of Energy, Office of Basic Energy Sciences. Tula Paudel thanks Andrey Zatukeyav and John Perkins for invaluable suggestions and useful discussions.

APPENDIX: EXPERIMENTAL PHASE BOUNDARY DATA

TABLE III. Experimental phase boundaries determined using lever rule and intercept/disappearing phase methods for different compositions in the Co-Zn-O system prepared at various temperatures. Experimental phase boundaries determined for samples of various compositions in the Rh-Zn-O system, prepared at 975 °C, are also included.

Temperature[a] (°C)	Overall specimen[b] composition $A/(A+B)$	Wt % wurtzite by Rietveld refinement	Lever rule[c] boundary, $A/(A+B)$	Intercept method boundary, $A/(A+B)$
390 (Co-Zn-O)	0.633	3.8 ± 0.7	0.66 ± 0.01	–
450 (Co-Zn-O)	0.633	4.1 ± 0.7	0.66 ± 0.01	–
500 (Co-Zn-O)	0.08	85.8 ± 1.0	0.57 ± 0.2	0.68
	0.12	81.3 ± 1.3	0.65 ± 0.1	
	0.16	78.2 ± 1.5	0.73 ± 0.1	
	0.633	3.8 ± 0.6	0.66 ± 0.01	
	0.667	2.6 ± 0.7	0.68 ± 0.01	
	0.767	0	..	
	0.80	0	..	
			Ave.[d] 0.66 ± 0.06	

TABLE III. (*Continued.*)

Temperature[a] (°C)	Overall specimen[b] composition $A/(A+B)$	Wt % wurtzite by Rietveld refinement	Lever rule[c] boundary, $A/(A+B)$	Intercept method boundary, $A/(A+B)$
575 (Co-Zn-O)	0.633	5.7 ± 0.6	0.67 ± 0.01	—
650 (Co-Zn-O)	0.08	88.4 ± 0.8	0.69 ± 0.2	0.73
	0.12	83.8 ± 1.1	0.74 ± 0.1	
	0.16	79.1 ± 1.4	0.76 ± 0.1	
	0.633	7.0 ± 1.0	0.68 ± 0.01	
	0.70	1.8 ± 0.2	0.71 ± 0.01	
	0.733	1.2 ± 0.2	0.74 ± 0.01	
	0.767	0.2 ± 0.1	0.77 ± 0.01	
	0.80	0	–	
			Ave. 0.73 ± 0.03	
800 (Co-Zn-O)	0.08	91.4 ± 0.6	0.65 ± 0.3	0.76
	0.12	88.1 ± 0.8	0.81 ± 0.3	
	0.16	82.1 ± 1.2	0.77 ± 0.2	
	0.633	15.0 ± 1.2	0.74 ± 0.01	
	0.667	16.1 ± 0.8	0.79 ± 0.01	
	0.70	4.3 ± 0.6	0.73 ± 0.01	
	0.733	2.4 ± 0.5	0.75 ± 0.01	
	0.767	0.8 ± 0.1	0.77 ± 0.01	
	0.80	0	–	
			Ave. 0.75 ± 0.05	
975 (Rh-Zn-O)	0.57	5.3 ± 0.4	0.66 ± 0.02	0.65
	0.59	3.9 ± 0.3	0.66 ± 0.01	
	0.62	1.9 ± 0.2	0.65 ± 0.01	
			Ave. 0.66 ± 0.006	

[a]For Zn-Co-O the temperature indicates the sintering and quench temperature. For Zn-Rh-O the temperature indicates the sintering temperature (samples were slow cooled).
[b]A is Co or Rh, and B is Zn, as in A_2BO_4.
[c]For the low Co/(Zn + Co) compositions, error is larger in Lever rule determination of the spinel phase boundary owing to its sensitivity to the exact location of the boundary between the wurtzite and two-phase regions.
[d]Uncertainties on the average values reflect standard deviations.

[1]H. Raebiger, S. Lany, and A. Zunger, Phys. Rev. B **76**, 045209 (2007).
[2]S. Lany, J. Osorio-Guillén, and A. Zunger, Phys. Rev. B **75**, 241203 (2007).
[3]S. Lany and A. Zunger, Phys. Rev. Lett. **98**, 045501 (2007).
[4]M. F. A. Harold and J. Frost, *The Transition-metal Carbides: ZrC and TiC*, 1st ed. (Pergamon Press, Oxford, 1982), Chap. 11.
[5]M. Straumanis, C. Faunce, and W. James, Acta Metall. **15**, 65 (1967).
[6]V. A. Gubanov, A. L. Ivanovsky, and V. P. Zhukov, *Electronic Structure of Refractory Carbides and Nitrides* (Cambridge University Press, Cambridge, 1994).
[7]Another widely used way of writing the spinel chemical formula is AB_2O_4. Here, we choose to use A_2BO_4 following Zhang and Zunger[8] mainly because the work presented here is part of a larger project that treats all A_2BX_4 compounds (not only spinels) in different structure types including Olivine Fe_2SiO_4, β-K_2SO_4 La_2CuO_4 for which A_2BX_4 is the generally used notation. Further it is to be noted that A_2BO_4 notation is common for spinels with formal cation valencies $Z_A = 2$ and $Z_B = 4$ such as Mg_2TiO_4.[9]
[8]X. Zhang and A. Zunger, Adv. Funct. Mater. **20**, 1944 (2010).
[9]B. A. Wechsler and A. Navrotsky, J. Solid State Chem. **55**, 165 (1984).
[10]P. Watson, M. V. Hove, and K. Hermann, *Collection of Phase Diagram*, Vol. 3.0 (National Institute of Standards and Technology, Gaithersburg, MD, 2010).
[11]H. S. C. O'Neill and A. Navrotsky, Am. Mineral. **68**, 181 (1983).
[12]V. Stevanović, M. d'Avezac, and A. Zunger, *Universal Electrostatic Origin of Cation Ordering in* A_2BO_4 *Spinel Oxides* (unpublished).
[13]R. Dieckmann and H. Schmalzried, Ber. Bunsen-Ges. Phys. Chem. **81**, 415 (1977).
[14]R. Dieckmann and H. Schmalzried, Ber. Bunsen-Ges. Phys. Chem. **81**, 344 (1977).
[15]For example, occupying $8b(3/8,3/8,3/8)$ position with metal ion (M), the two-coordination shells will be M-$(A_4O_4)(A_{12}B_4)$. Similarly occupying $16c(0,0,0)$, lead to M-$(B_2O_6)(A_6)$ coordination shell. Other lower symmetry Wyckoff position convert themselves

to high symmetry Wyckoff positions for certain value of x, y, z and high-symmetry Wyckoff position other then 8a, 16d lead to nonideal bonding. Other asymmetrical position are unlikely to produce favorable bonding leading to occupation of interstitial positions.

[16]C.-J. Ting and H.-Y. Lu, J. Am. Ceram. Soc. **82**, 841 (1999).

[17]R. J. Bratton, J. Am. Ceram. Soc. **52**, 417 (1969).

[18]T. R. Paudel, A. Zakutayev, M. d'Avezac, S. Lany, and A. Zunger, *Doping Rules and Doping Prototypes in* A_2BO_4 *Spinels* (unpublished).

[19]M. Lenglet, R. Guillamet, J. Durr, and D. Gryffroy, and R. Vandenberghe, Solid State Commun. **74**, 1035 (1990).

[20]H. Eba and K. Sakurai, J. Solid State Chem. **178**, 370 (2005).

[21]D. Ko, J. Solid State Chem. **163**, 259 (2002).

[22]N. K. Radhakrishnan and A. B. Biswas, Phys. Status Solidi A **44**, 45 (1977).

[23]G. Materlik, C. Sparks, and K. Fischer, eds., *Resonant Anomalous X-Ray Scattering: Theory and Applications* (North Holland, New York, 1994).

[24]B. B. Nelson-Cheeseman, R. Chopdekar, J. Iwata, M. Toney, E. Arenholz, and Y. Suzuki, Phys. Rev. B **82**, 144419 (2010).

[25]S. Lany, Y.-J. Zhao, C. Persson, and A. Zunger, Appl. Phys. Lett. **86**, 042109 (2005).

[26]P. E. Blöchl, Phys. Rev. B **50**, 17953 (1994).

[27]J. P. Perdew, K. Burke, and M. Ernzerhof, Phys. Rev. Lett. **77**, 3865 (1996).

[28]G. Kresse and J. Furthmller, Comput. Mater. Sci. **6**, 15 (1996).

[29]J. Paier, R. Hirschl, M. Marsman, and G. Kresse, J. Chem. Phys. **122**, 234102 (2005).

[30]S. L. Dudarev, G. A. Botton, S. Y. Savrasov, C. J. Humphreys, and A. P. Sutton, Phys. Rev. B **57**, 1505 (1998).

[31]H. J. Monkhorst and J. D. Pack, Phys. Rev. B **13**, 5188 (1976).

[32]S. Lany and A. Zunger, Phys. Rev. B **78**, 235104 (2008).

[33]S. Baroni and R. Resta, Phys. Rev. B **33**, 7017 (1986).

[34]D. Cox and A. Wilkinson, in *Resonant Anomalous X-Ray Scattering, Theory and Applications*, edited by G. Materlik, C. Sparks, and K. Fischer (North Holland, New York, 1993), p. 195.

[35]B. Cullity and S. Stock, *Elements of X-Ray Diffraction*, 3rd ed. (Prentice Hall, Englewood Cliffs, NJ, 2001).

[36]V. Stevanović, M. d'Avezac, and A. Zunger, Phys. Rev. Lett. **105**, 075501 (2010).

[37]R. J. Hill, J. R. Craig, and G. V. Gibbs, Phys. Chem. Miner. **4**, 317 (1979).

[38]P. Porta, J. Solid State Chem. **121**, 372 (1996).

[39]K. Krezhov and P. Konstantinov, J. Phys. Condens. Matter **4**, L543 (1992).

[40]N. Bahlawane, P. A. Premkumar, J. Feldmann, and K. Kohse-Höinghaus, Chem. Vap. Deposition **13**, 118 (2007).

[41]J. Perkins, T. Paudel, A. Zakutayev, P. Ndione, P. Parilla, S. Lany, D. Ginley, A. Zunger, N. Perrry, T. Mason, J. Bettinger, Y. Shi, and M. Toney, *Strategies for Hole Doping Ternary Oxides: Enhancing p-type Conductivity in Cobalt Oxide Spinels* (unpublished).

[42]M. Dekkers, G. Rijnders, and D. H. A. Blank, Appl. Phys. Lett. **90**, 021903 (2007).

[43]K. Petrov, L. Markov, and R. Ioncheva, J. Mater. Sci. Lett. **4**, 711 (1985).

[44]J. Robin, Ann. Chim. (Paris) **10**, 389 (1955).

[45]D. Wagman, *The NBS Tables of Chemical Thermodynamic Properties: Selected Values for Inorganic and C and C Organic Substances in SI Units* (American Chemical Society and the American Institute of Physics for the National Bureau of Standards, New York, Washington, DC, 1982).

[46]R. Dieckmann, Z. Phys. Chem. NF **107**, 189 (1977).

[47]E. Woermann, J. Inorg. Nucl. Chem. **32**, 1455 (1970).

[48]E. Aukurst and A. Muan, J. Am. Ceram. Soc. **46**, 511 (1963).

[49]M. Chen, B. Hallstedt, and L. J. Gauckler, J. Phase Equilib. **24**, 212 (2003).

[50]K. Mocala, Phys. Chem. Miner. **19**, 89 (1992).

[51]G. Kale, S. Pandit, and K. Jacob, Trans. Jpn. Inst. Met. **29**, 125 (1988).

[52]A. D. Pelton, H. Schmalzried, and J. Sticher, Ber. Bunsen-Ges. Phys. Chem. **83**, 241 (1979).

[53]H. Mizoguchi, M. Hirano, S. Fujitsu, T. Takeuchi, K. Ueda, and H. Hosono, Appl. Phys. Lett. **80**, 1207 (2002).

[54]A. Banerjee and Z. Singh, J. Solid State Electrochem. **13**, 1201.

[55]B. Hallstedt, J. Am. Ceram. Soc. **75**, 1497 (1992).

[56]R. K. Datta and R. Roy, J. Am. Ceram. Soc. **51**, 297 (1968).

[57]A. Navrotsky, B. A. Wechsler, K. Geisinger, and F. Seifert, J. Am. Ceram. Soc. **69**, 418 (1986).

[58]R. Ahuja, J. M. Osorio-Guillen, J. S. D. Almeida, B. Holm, W. Y. Ching, and B. Johansson, J. Phys. Condens. Matter **16**, 2891 (2004).

[59]R. Roy, V. G. Hill, and E. F. Osborn, J. Am. Chem. Soc. **74**, 719 (1952).

[60]S. Yoshioka, H. Hayashi, A. Kuwabara, F. Oba, F. Matsunaga, and I. Tanaka, J. Phys. Condens. Matter **19**, 346211 (2007).

[61]H. S. C. O'Neil and A. Navrotsky, Am. Mineral. **69**, 733 (1984).